Astron. Astrophys. 358, 144–153 (2000)

ASTRONOMY AND ASTROPHYSICS

# Studies of binary star cluster candidates in the bar of the LMC

## I. SL 353 and SL 349⋆

**A. Dieball**[1], **E.K. Grebel**⋆⋆[2], **and C. Theis**[3]

[1] Sternwarte der Universität Bonn, Auf dem Hügel 71, 53121 Bonn, Germany
[2] University of Washington, Department of Astronomy, Box 351580, Seattle, WA 98195-1580, USA
[3] Institut für Theoretische Physik und Astrophysik der Universität Kiel, 24098 Kiel, Germany

Received 22 December 1999 / Accepted 27 March 2000

**Abstract.** We present a detailed study of the cluster pair SL 353 & SL 349. This candidate binary cluster is located at the north-western rim of the LMC bar. Based on photometric data we find that both clusters are coeval with an age of $550\pm100$ Myr. We use the Ca II triplet in the spectra of individual red giants to derive radial velocities. Both components of the binary cluster candidate show very similar mean velocities ($\approx 274\pm10\,\mathrm{km\,s^{-1}}$ for SL 349 and $\approx 279\pm4\,\mathrm{km\,s^{-1}}$ for SL 353) while the field stars show lower velocities ($\approx 240\pm19\,\mathrm{km\,s^{-1}}$). These findings suggest a common origin of the two clusters from the same GMC. In this sense the cluster pair may constitute a true binary cluster. We furthermore investigate the stellar densities in and around the star clusters and compare them with isopleths created from artificial, interacting as well as non-interacting star clusters. Gravitational interaction leads to a distortion which can also be found in the observed pair.

**Key words:** stars: Hertzsprung–Russel (HR) and C-M diagrams – stars: kinematics – galaxies: clusters: individual: SL 353, individual: SL 349 – galaxies: Magellanic Clouds

### 1. Introduction

The Magellanic Clouds offer the unique possibility to study star clusters in general and binary clusters in particular. These two companion galaxies are close enough to resolve single stars, but distant enough to make the detection of close pairs of star clusters an easy task. About a decade ago, Bhatia & Hatzidimitriou (1988), Hatzidimitriou & Bhatia (1990), and Bhatia et al. (1991) surveyed the Magellanic Clouds in order to catalogue binary cluster candidates. To qualify as a binary cluster candidate, the maximum projected centre-to-centre separation of the components of a pair was chosen to be $\approx 1\farcm3$, which corresponds to $\approx 19$ pc in the LMC if a distance modulus of 18.5 mag is adopted. A binary cluster with larger separation may become detached by the external tidal forces while shorter separations may lead to mergers (Sugimoto & Makino 1989, Bhatia 1990). The number of chance-pairs of objects uniformly distributed in space can be estimated adopting a formula presented by Page (1975): Roughly half of the pairs found may be explained by mere chance line-up. This suggests that at least a subset of them must be true binary clusters, i.e., clusters that are formed together and/or may interact or even be gravitationally bound.

Depending on their masses and separations binary clusters will eventually merge or become detached. At one stage during the merger process the former binary cluster could have one single but elliptical core (Bhatia & McGillivray 1988). Recently de Oliveira et al. (2000) performed numerical simulations of star cluster encounters which could represent a possible scenario to explain the ellipticities found in several star clusters in the Magellanic Clouds.

Star clusters form in giant molecular clouds (GMCs), but the details of cluster formation are not yet understood (Elmegreen et al. 1999). Fujimoto & Kumai (1997) suggest that binary or multiple star clusters form through strong, oblique collisions between massive gas clouds in high-velocity random motion, resulting in compressed sub-clouds revolving around each other. Since the components of a cluster pair formed together, they should be coeval or at least have a small age difference compatible with cluster formation time scales. Binary clusters are expected to form more easily in galaxies like the Magellanic Clouds, whereas in the Milky Way the required large-scale high-velocity random motions are lacking. Indeed only few binary open cluster candidates and no globular cluster pairs are known in our Galaxy (see for example Subramaniam & Sagar 1999). However, binary globular clusters are not expected to survive the gravitational forces of the Milky Way (Surdin 1991).

In case of tidal capture two clusters would be gravitationally bound, but age differences are likely. Encounters of clusters can be traced using isodensity maps (de Oliveira et al. 1998, Leon et al. 1999). Though van den Bergh (1996) suggests that tidal capture becomes more probable in dwarf galaxies like the Magellanic Clouds with small velocity dispersion of the cluster system, Vallenari et al. (1998) estimated a cluster encounter rate

*Send offprint requests to*: A. Dieball (adieball@astro.uni-bonn.de)

⋆ Based on observations taken at the European Southern Observatory, La Silla, Chile.

⋆⋆ Hubble fellow

of $dN/dt \sim 1 \cdot (10^9\mathrm{yr})^{-1}$. This makes tidal capture of young clusters very unlikely.

The formation of low-mass star clusters tends to proceed hierarchically in large molecular complexes over several $10^7$ years (e.g., Efremov & Elmegreen 1998). Leon et al. (1999) suggest that in these groups the cluster encounter rate is higher and thus tidal capture is more likely: Binary clusters are not born together as a pair with similar ages but are formed later through gravitational capture. An observational test of this scenario would require the detection of evidence of tidal interactions between clusters, whose age differences need to be compatible with the survival times of GMCs.

Another binary cluster formation scenario is introduced by Theis (1998) and Ehlerová et al. (1997): Exploding supernovae close to the centre of a GMC sweep up the outer cloud material within a few Myrs and accumulate it in the shell. The large amount of matter makes the shell prone to gravitational fragmentation and may eventually lead to the formation of many open cluster-like associations (Theis et al. 1997, Ehlerová et al. 1997). In case of a dense ambient medium outside the cloud or a very massive original molecular cloud the shell can be strongly decelerated resulting in a gravitationally bound system of fragments or stars which can recollapse. A galactic tidal field acting on this recollapsing shell can split it into two or more large clusters, thus forming coeval twin globulars (Theis 1998). These clusters may stay together for a long time, though they are gravitationally unbound. The evolution of their spatial separation mainly depends on the shape of the shock front at the time of fragmentation.

We are studying binary cluster candidates in the Magellanic Clouds to investigate whether the cluster pairs may be of common origin and if they show evidence for interaction. While it is so far impossible to measure true, deprojected distances between apparent binary clusters, an analysis of their properties can give clues to a possible common origin.

The binary cluster candidate SL 353 (or BRHT 33b, see Bhatia et al. 1991) and SL 349 (BRHT 33a) is located in the outer western part of the LMC bar. Based on integrated colours, Bica et al. (1996) suggest that SL 353 & SL 349 are coeval clusters of SWB type V (Searle et al. 1980) which is in agreement with the findings of Vallenari et al. (1998). Leon et al. (1999) suggest that the two clusters may even be physically connected. Based on ages for a large sample of star clusters, derived on the base of integrated colours, Bica et al. (1996) propose an age gradient of the LMC bar. Younger clusters are predominantly found in the eastern part, while older clusters of SWB type III and higher are concentrated to its western end.

This paper is organized as follows. In Sect. 2 we describe the photometric data in general. Stellar density maps are presented in Sect. 3. The following section describes the colour magnitude diagrams (CMD) for the components of the cluster pair. Ages for each cluster are derived and compared with previous studies. The spectroscopic data are described in Sect. 5, and radial velocities are derived in Sect. 6. A comparison of the observed isopleths with simulated ones for interacting and non-interacting star clusters is given in Sect. 7. In the last Sect. 8 we summarize and discuss the results.

**Table 1.** Observing log

| Filter | Exp.time [s] | Seeing [″] |
|---|---|---|
| Gunn $g$ | 600 | 1.6 |
| Gunn $g$ | 60 | 1.4 |
| Gunn $g$ | 40 | 1.4 |
| Gunn $i$ | 240 | 1.1 |
| Gunn $i$ | 20 | 1.2 |

**Table 2.** Transformation coefficients

| Filter | $c_i$ | $z_i$ [mag] | $a_i$ [mag] |
|---|---|---|---|
| Gunn $g$ | $-0.060 \pm 0.006$ | $1.685 \pm 0.030$ | $0.206 \pm 0.019$ |
| Gunn $i$ | $0.051 \pm 0.003$ | $2.439 \pm 0.016$ | $0.081 \pm 0.010$ |

## 2. Photometric observations and data reduction

The data were obtained on March 22, 1994, with EFOSC 2 at the ESO/MPI 2.2 m telescope at La Silla. A $1024 \times 1024$ coated Thomson 31156 chip (ESO #19) was used with a pixel scale of $0\farcs34$ resulting in a field of view of $5\farcm8 \times 5\farcm8$. These data were obtained with the Gunn $g$ (which is similar to Washington $M$) and Gunn $i$ (corresponding to Washington $T2$) filters used at the 2.2 m telescope. An observing log is given in Table 1. During standard image reduction with MIDAS we noticed flatfielding problems near the edges of the exposures. Thus, each image was cut out resulting in a field of view of $4\farcm3 \times 3\farcm5$. An image of the binary cluster candidate is shown in Fig. 1.

Profile fitting photometry was carried out with DAOPHOT II (Stetson 1991) running under MIDAS.

The photometry was transformed using the standard fields around SA 110 and SA 98 (Geisler 1990) observed in the same night.

We applied the following transformation relations:

$$g - G = z_G + a_G \cdot X + c_G \cdot (G - I)$$
$$i - I = z_I + a_I \cdot X + c_I \cdot (G - I),$$

where $X$ is the mean airmass during observation, capital letters represent standard magnitudes and colours, and lower-case letters denote instrumental magnitudes after normalizing to an exposure time of 1 sec. The resulting colour terms $c_i$, zero points $z_i$ and atmospheric extinction coefficients $a_i$ are listed in Table 2.

## 3. Stellar density maps

The cluster pair SL 353 & SL 349 (see Fig. 1) is located in the inner northwestern part of the LMC at the outer rim of the bar. The projected distance between the clusters' centres is $1\farcm24$. Assuming a distance modulus of $m - M = 18.5$ mag (Westerlund 1997) this corresponds to 18.1 pc. According to Sugimoto & Makino (1989) this is close to the maximum separation at

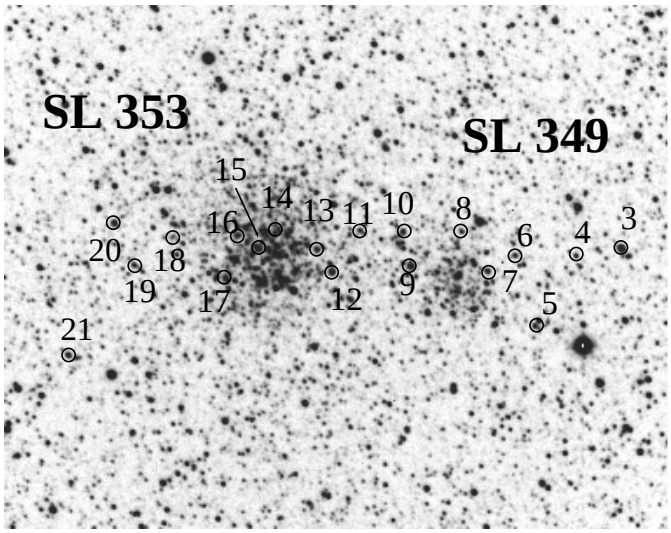


**Fig. 1.** Gunn $i$-image of the cluster pair SL 353 & SL 349. North is up and east to the left. The field of view of this image is $4\farcm3 \times 3\farcm5$. These clusters are located at the outer northwestern rim of the LMC bar. For the stars marked with circles also spectroscopic data were obtained (see Sect. 5)

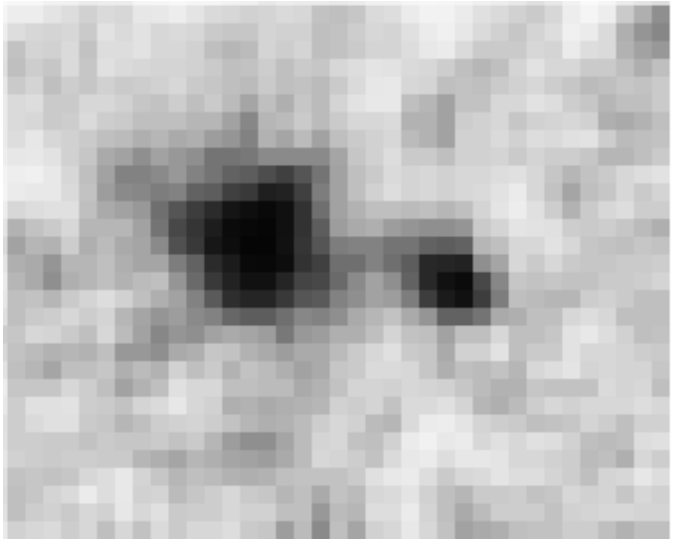

**Fig. 2.** Star density map of SL 353 & SL 349. The star density between the cluster pair is enhanced. Note the distortion of SL 349 towards the bigger cluster SL 353. Similar distortions are seen around the more massive cluster

which a binary cluster is still stable and will not be detached by the outer tidal forces of the LMC.

We investigate the stellar density distribution in and around the clusters by counting the number of stars in square cells of 20 pixels length (corresponding to $6\farcs8$ or 1.7 pc). To make density structures and thus possible signs of interaction better visible we applied a $3 \times 3$ average filter for image smoothing. The procedure is described in more detail in Dieball & Grebel (1998).

The stellar density map is presented in Fig. 2. The star density between the two clusters is enhanced compared to the surrounding field density. The enhancement is about 3 $\sigma$ above the field background and thus significant at a $\approx 99\%$-level. In addition, the smaller cluster SL 349 seems to be warped towards SL 353. Also the density profile of SL 353 shows distortions: we see smaller arcs of enhanced density reaching to the north and south, and also to the northeast. Whether these features might be tidal tails due to an interaction with the LMC tidal field or even due to an interaction with the smaller companion SL 349, as suggested by Leon et al. (1999), is hard to decide.

## 4. Colour magnitude diagrams and isochrone fitting

To derive the CMDs for each cluster we cut out a circular area centred around the optical centre of each cluster. The radius was chosen to be 100 pixels (corresponding to $34''$ or 8.3 pc) for SL 349, and 120 pixels (corresponding to $40\farcs8$ or 9.9 pc) for SL 353. An investigation of the star density plots suggests that most cluster stars are located inside the chosen areas. The cluster CMDs were compared with the CMD of the surrounding field and a statistical field star subtraction was applied to clear the cluster CMDs from contaminating field stars which might affect the age determination. To take into account the different area sizes of the regions covered by the clusters and the surrounding field we weighted the field star subtraction with field sizes.

**Table 3.** Number of foreground stars towards the LMC calculated from the data of Ratnatunga & Bahcall (1985), scaled to our field of view of $4\farcm3 \times 3\farcm5$

| | apparent visual magnitude range | | | | |
|---|---|---|---|---|---|
| colour range | 13–15 | 15–17 | 17–19 | 19–21 | 21–23 |
| $B-V<0.8$ | 0.6 | 1.3 | 1.4 | 2.9 | 2.7 |
| $0.8<B-V<1.3$ | 0.2 | 1.2 | 2.4 | 1.9 | 3.3 |
| $1.3<B-V$ | 0.0 | 0.3 | 1.7 | 5.7 | 13.1 |

We derived ages for the clusters by comparing the CMDs with isochrones which are based on the stellar models of the Geneva group (Schaerer et al. 1993). The isochrones were transformed to the Washington system by Roberts & Grebel (1994).

A distance modulus of 18.5 mag (Westerlund 1997) was adopted. We assumed a metallicity of Z = 0.008 corresponding to $[Fe/H] \approx -0.3$ dex which was found by various authors for the young field star population (e.g., Russell & Bessell 1989, Luck & Lambert 1992, Russell & Dopita 1992, Thévenin & Jasniewicz 1992).

Galactic field stars may contaminate our observed area. In order to assess whether foreground stars might affect our age determination we compare our CMDs with the number of galactic field stars towards the LMC estimated by Ratnatunga & Bahcall (1985). In Table 3 we present their counts scaled to our field of view of $4\farcm3 \times 3\farcm5$. As can be seen, the number of expected foreground stars is small, and we do not expect an influence on our age determination.

The CMDs of the two clusters and the surrounding field and the isochrone fitting are described in more detail in the following.

*SL 353:* The CMD of this cluster is shown in Fig. 3, upper left plot. Open and filled data points represent all stars which are located inside a radius of $40\farcs8$. After statistical field star subtraction only the open circles remain. The CMD shows a wide blue main sequence. The width of the main sequence is caused in part by photometric errors (average seeing $1\farcs4$) and crowding. Also a pronounced red clump of He-core burning stars and some red giants can be seen. Most red clump stars remain after field star subtraction, an indication of the intermediate age of this cluster. The ratio of red clump stars in the cluster and in the surrounding field is approximately 3:1. The small open circles denote the stars that can be found inside an annulus of $17''$ where crowding is most severe. The width of the main sequence and the scatter of the red giants is caused in part by this crowding. Overplotted on the CMD are several possible isochrones. An isochrone resulting in an age of 500 Myr (upper line) gives a good fit to the apparent main sequence turnoff at $T2 \approx 18.5$ mag. However, the evolved stars are not well represented by this isochrone. Fitting the He-core burning giants results in higher ages of 630 Myr (middle line) or 800 Myr (lower line) but also underestimates the luminosity of the main sequence turnoff. Since the fit to the main sequence provides a lower age limit we adopt a mean age of 550$\pm$100 Myr for SL 353.

Such a discrepancy between the main sequence turnoff and red giants luminosities was noticed in the CMDs of various other LMC star clusters, two prominent examples are NGC 1866 and NGC 1850 (see Brocato et al. 1989, Lattanzio et al. 1991, Vallenari et al. 1994b, Brocato et al. 1994). Unresolved binary stars which could increase the luminosity of the main sequence turnoff were proposed as one explanation. Other possibilities include blue stragglers and/or rotation (Grebel et al. 1996). Vallenari et al. (1994a) point out that no direct evidence for a significant population of binary stars could be found, though the detection of close binary stars in the Magellanic Clouds is difficult if not impossible. Lattanzio et al. (1991) was able to solve the problem by taking into account unresolved binaries as well as semiconvection. Their simulated CMDs then gave a good representation of the observed ones.

*SL 349:* Fig. 3, upper right plot, presents the CMD of SL 349. Again, large and small open circles denote stars that remain after field star subtraction. SL 349 is the smaller one of the cluster pair, as can also be seen from the sparse main sequence and red giant clump. The small, open circles represent the stars located inside an inner, crowded annulus of $13\farcs6$. Fitting an isochrone to the apparent main sequence turnoff ($T2 \approx 18.5$ mag) results in an age of 500 Myr (upper line). However, note again the pronounced red clump that is present in the CMD. We find approximately twice the amount of red clump stars in the cluster than in the field, scaled to the same area. Fitting isochrones to the core-He-burning red giants results in somewhat higher ages than isochrone fits that take into account the apparent main sequence turnoff, namely 630 Myr (middle line) or 800 Myr (lower line). We adopt the same age of 550$\pm$100 Myr for SL 349 that we already found for SL 353.

Our findings are in agreement with former age determinations: Vallenari et al. (1998) found from CMDs a very similar age of 500$\pm$100 Myr for both clusters. Based on integrated colours, Bica et al. (1996) suggest that the clusters are of somewhat older SWB type V (800–2000 Myr). Studying the stellar content of proposed binary clusters in the LMC, Kontizas et al. (1989) found the older cluster pairs in their sample, among them SL 353 & SL 349, younger than 600 Myr, which agrees with our findings and those of Vallenari et al. (1998).

*The surrounding field:* The CMD of the surrounding field is shown in the lower diagram of Fig. 3. A mixture of populations of different ages can be found around the cluster pair. The CMD shows a bright blue main sequence and a few red supergiants which represent the young population. The intermediate age populations show up through the pronounced red clump of He-core burning stars and the red giants. Distinct young populations cannot be distinguished, but the overplotted isochrones are supported by corresponding supergiants. Fainter main sequence stars and red giants are plotted with smaller data points to keep the isochrones recognizable. The dotted isochrone fits to the brightest main sequence stars and to some supergiants, resulting in an age of 32 Myr. Also the 63 Myr isochrone (short dashed line) gives a good representation of the few red supergiants. We see again a few bright supergiants at $T2 \approx 16.5$ mag which can be fitted with a 200 Myr isochrone (long dashed line). Between 200 Myr and 400 Myr (solid line) the star density along the subgiant branch seems to be lower, indicating a possible decrease in the field star formation rate, but increases again along and below the 400 Myr isochrone (solid line).

Since the main sequences in the CMDs show a large scatter, it is impossible to derive a reddening via isochrone fitting. Thus, we adopt a reddening of $E_{B-V} = 0.1$ mag, corresponding to $E_{M-T2} = 0.15$ mag (see Grebel & Roberts 1995, their Table 5, for the transformation of extinctions in different filter systems), as suggested from the reddening maps of Schwering & Israel (1991).

## 5. Spectroscopic data and their reduction

In order to derive radial velocities, multi-object spectra (MOS) for 22 stars in and around the star clusters SL 535 & SL 349 were obtained on February 09, 1995, using EMMI RILD at the ESO/NTT at La Silla. A TEK $2048 \times 2048$ chip (ESO #36) was used with a pixel scale of $0\farcs27$. The resulting field of view is $9\farcm2 \times 8\farcm6$. Slit masks are prepared at the NTT during observation, the punch field covers $5' \times 8'$. Only 19 stars out of 22 for which spectra were obtained are located inside the smaller field of view of the photometric data ($4\farcm3 \times 3\farcm5$). They are marked in Fig. 1. The spectra were taken with grism #6 which covers a wavelength range of 6000 to 8300 Å when the slits are centred on the CCD chip, and provides a dispersion of 1.2 Å per pixel. The brightest stars in both clusters are red giants (see Sect. 4), so we chose to obtain spectra of red giants at the Ca II triplet at $\lambda =$ 8498 Å, 8662 Å and 8542 Å (see e.g. Olszewski et al. 1991). The wavelength coverage of the MOS depends on the position of the slits with respect to the centre of the CCD. In order to reach the Ca II lines the X-position of the slits was shifted about $\approx 2\farcm5$ or $\approx 530$ pixels resulting in a wavelength coverage of 6500 to

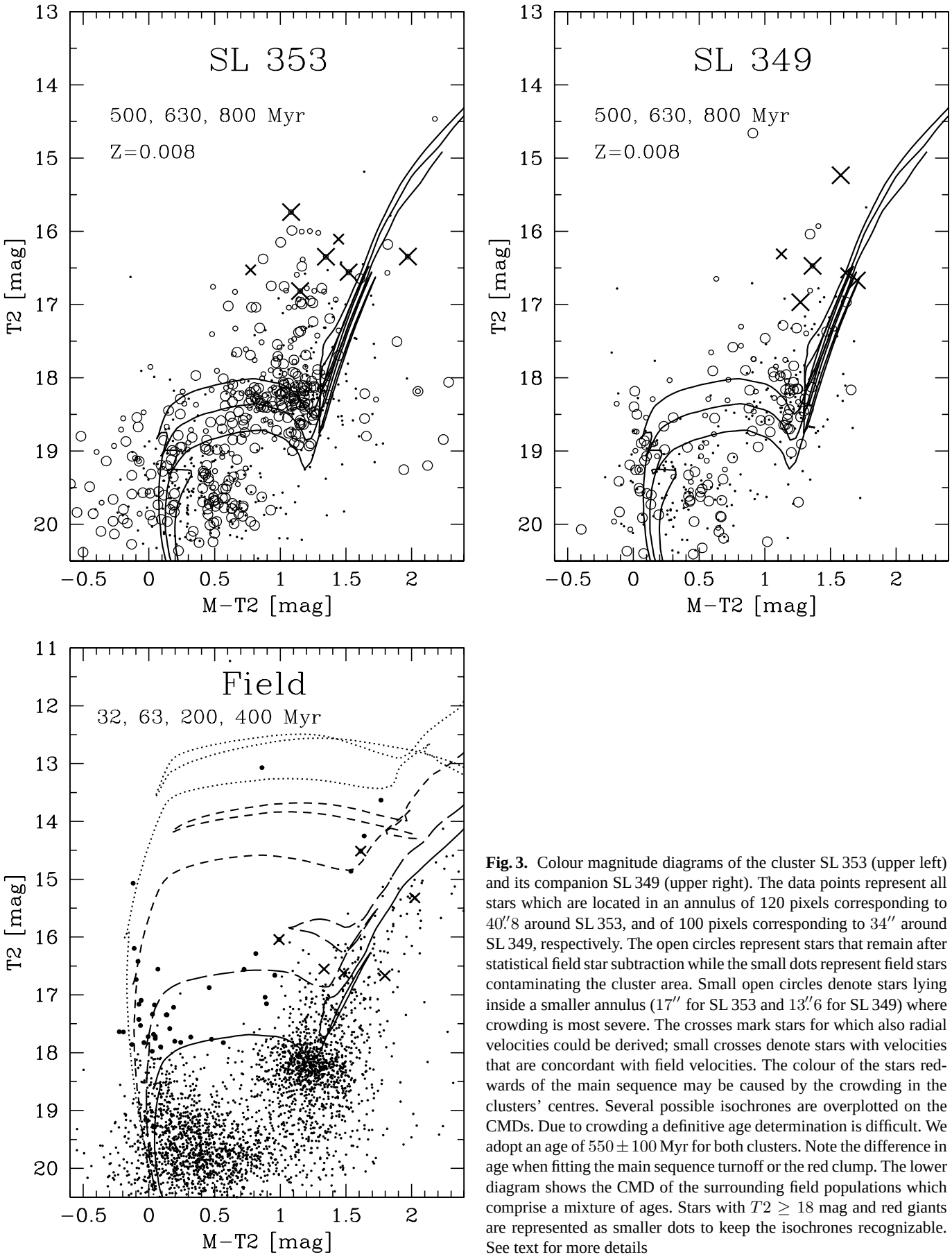


**Fig. 3.** Colour magnitude diagrams of the cluster SL 353 (upper left) and its companion SL 349 (upper right). The data points represent all stars which are located in an annulus of 120 pixels corresponding to $40\farcs8$ around SL 353, and of 100 pixels corresponding to $34''$ around SL 349, respectively. The open circles represent stars that remain after statistical field star subtraction while the small dots represent field stars contaminating the cluster area. Small open circles denote stars lying inside a smaller annulus ($17''$ for SL 353 and $13\farcs6$ for SL 349) where crowding is most severe. The crosses mark stars for which also radial velocities could be derived; small crosses denote stars with velocities that are concordant with field velocities. The colour of the stars redwards of the main sequence may be caused by the crowding in the clusters' centres. Several possible isochrones are overplotted on the CMDs. Due to crowding a definitive age determination is difficult. We adopt an age of $550 \pm 100$ Myr for both clusters. Note the difference in age when fitting the main sequence turnoff or the red clump. The lower diagram shows the CMD of the surrounding field populations which comprise a mixture of ages. Stars with $T2 \geq 18$ mag and red giants are represented as smaller dots to keep the isochrones recognizable. See text for more details

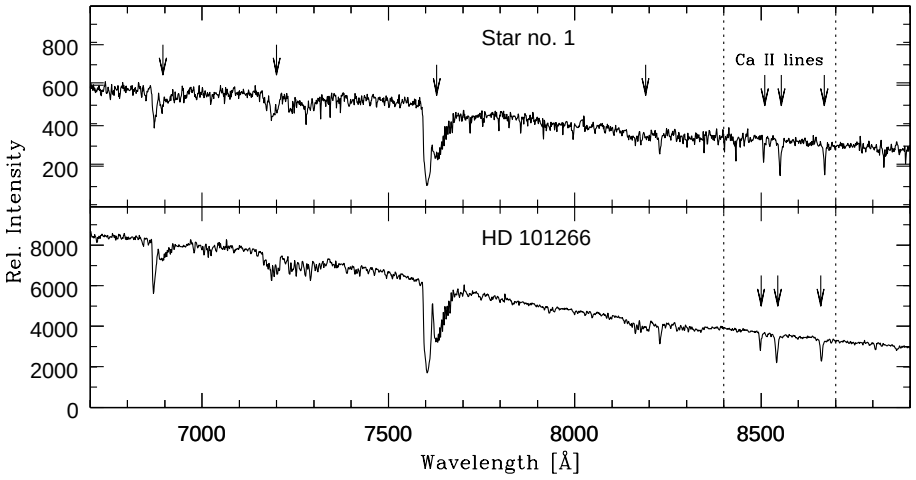


**Fig. 4.** The upper panel shows the spectrum of the Star no. 1 while the lower panel shows the spectrum of the radial velocity standard star HD 101266. Strong night sky absorption lines are marked with arrows (only in the upper panel): The two sharp peaks at $\lambda = 6867$ Å and $\lambda = 7594$ Å denote to the $O_2$ B-band and $O_2$ A-band, the other two more extended bands starting at $\lambda = 7186$ and 8164 Å, respectively, are caused by atmospheric water vapor. For the crosscorrelation only the wavelength range between the dotted lines was used. The Ca II triplet can be clearly seen in both spectra

**Table 4.** Observing log of the spectroscopic data

| Object | $\alpha_{2000}$ [h m s] | $\delta_{2000}$ [° ′ ″] | Exp.time [s] | velocity [km s$^{-1}$] |
|---|---|---|---|---|
| SL 353/349 | 05 16 00 | −68 56 00.0 | 3600 | |
| HD 101266 | 11 38 50.73 | −45 21 45.3 | 30 | +20.6 |
| HD 111417 | 12 49 31.82 | −45 49 32.8 | 30 | −16.0 |
| HD 120223 | 13 49 06.56 | −43 44 00.1 | 30 | −24.1 |

9000 Å. The slit width was $\approx 1''$ (corresponding to 4 pixels). In the same night the radial velocity standard stars HD 101266, HD 111417, and HD 120223 were observed using the same slit mask. An observing log is given in Table 4. The velocities of the standard stars were taken from Evans (1967).

Data reduction was carried out using IRAF's `twodspec` and `onedspec` packages. We mainly followed the procedure for multislit spectroscopic reductions described in Ellingson (1989). Wavelength calibration was performed using He-Ar spectra obtained in the same night with the same slit mask.

## 6. Radial velocities

We derived the radial velocities for the 22 stars by crosscorrelating each spectrum with the spectra of the three standard stars listed in Table 4. An example is given in Fig. 4. The upper panel shows the spectrum of the Star no. 1 (which lies outside of the useful area of our imaging data) while the lower panel shows the spectrum of the radial velocity standard star HD 101266. The whole wavelength range covered by the grism is plotted. Strong atmospheric absorption lines are visible in both spectra. The sharp peak at $\lambda = 6867$ Å denotes the $O_2$ B-band, and the even stronger double peak at $\lambda = 7594$ Å belongs to the $O_2$ A-band (Turnshek et al. 1985). Two $H_2O$-bands are visible, starting at $\lambda = 7186$ and 8164 Å, respectively.

Using the IRAF task `fxcorr` in the package `rv` we applied a crosscorrelation between each programme and standard star spectrum. For this purpose we only need the Ca II lines. In Fig. 4 the region used for the crosscorrelation is marked with dotted lines. Table 5 gives an overview of the radial velocities for all observed stars. The velocities listed are the error weighted mean of the three velocities derived from the crosscorrelation between the programme and the three standard stars.

In Fig. 5 the spectra of all 22 programme stars are shown. We only plotted a wavelength range of 8350 Å to 8750 Å which includes the Ca II lines from which we derived the velocities. The two strongest lines of the Ca II triplet can be clearly seen in all spectra at $\approx 8670$ Å and $\approx 8550$ Å. The third and weakest line appears at $\approx 8500$ Å.

Star no. 8 is the faintest star of our sample and thus shows the noisiest spectrum (see Fig. 5), which is also responsible for the large error of the velocity (see Table 5). Also star no. 10 shows a somewhat noisy spectrum and has a higher $\sigma$. Stars no. 20 and 22 must be foreground stars since their velocities are small (14.4 km s$^{-1}$ and 84.3 km s$^{-1}$, respectively). The minor displacement of the Ca II lines can be clearly seen in Fig. 5. All other stars have velocities which indicate that they are LMC members (approximately 200–320 km s$^{-1}$, see e.g. Prévot et al. 1985, or Westerlund 1997). Stars no. 1 and 16 have velocities higher than 300 km s$^{-1}$. These two stars might be field stars having such a high velocity, or they may be variable or binary stars (see e.g. Fischer et al. 1993).

The programme stars are located in the field as well as in both clusters and in between the two clusters. It is striking that most stars located inside the cluster areas have higher velocities while (almost) all field stars show lower velocities (see Table 5). The components of our proposed binary cluster have very similar mean radial velocities of $\approx 274 \pm 10$ km s$^{-1}$ for SL 349 (stars no. 6, 8, 9, 10) and $\approx 279 \pm 4$ km s$^{-1}$ for SL 353 (stars no. 11, 12, 13, 14, 17). The mean velocity for both clusters is $\approx 277 \pm 7$ km s$^{-1}$. In contrast the investigated field stars have velocities of $\approx 240 \pm 19$ km s$^{-1}$. The errors given for these mean velocities are the standard deviations.

The expected internal velocity dispersion of a star cluster is of the order of only few km s$^{-1}$ (see, e.g., Westerlund 1997). However, since the mean error of one single velocity measurement is $\approx 6.6$ km s$^{-1}$ we do not state about the internal velocity dispersion of SL 349 or SL 353.

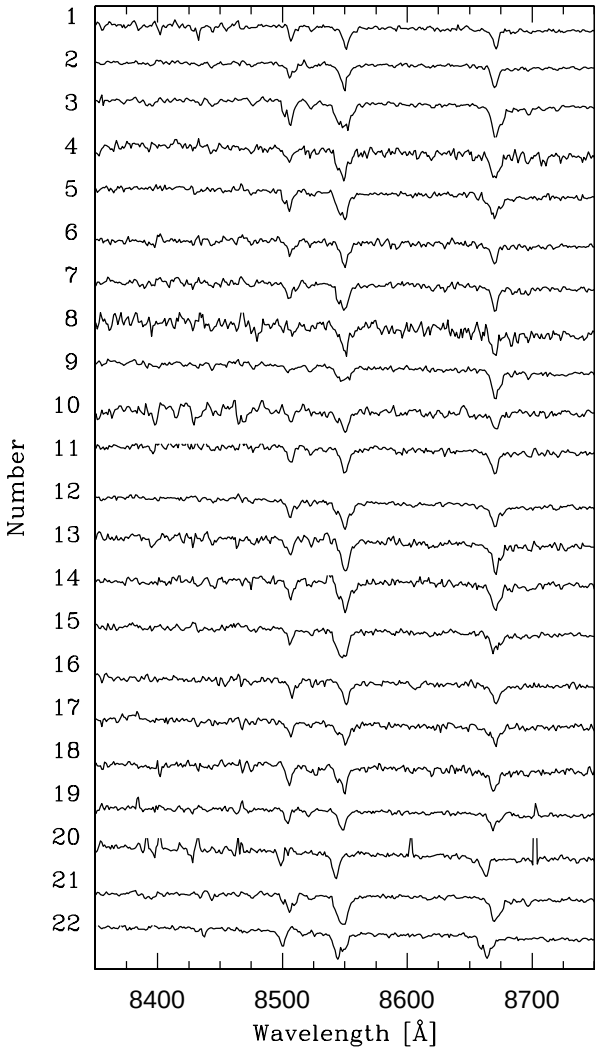


**Fig. 5.** Spectra of the stars no. 1 to 22. Only the wavelength range of 8350 Å to 8750 Å which includes the Ca II lines and which was used for the crosscorrelation is plotted. The Ca II triplet rest wavelenghts are at $\lambda = 8498$ Å, 8662 Å and 8542 Å. The Ca II lines for the stars no. 20 and 22 are less displaced compared to the other spectra which identifies them as galactic foreground stars. See text for more details

**Table 5.** Radial velocities of all 22 programme stars

| star no. | velocity [km s$^{-1}$] | $T2$ [mag] | $M-T2$ [mag] | comment |
|---|---|---|---|---|
| 1 | 313.7±3.1 | — | — | variable/binary? |
| 2 | 265.5±2.5 | — | — | field star |
| 3 | 268.5±3.7 | 14.52 | 1.61 | field star |
| 4 | 231.1±2.4 | 16.62 | 1.48 | field star |
| 5 | 232.7±2.9 | 16.31 | 1.12 | field star |
| 6 | 275.2±2.6 | 16.67 | 1.70 | cluster star |
| 7 | 248.7±3.2 | 16.57 | 1.62 | field star |
| 8 | 283.9±8.2 | 16.97 | 1.27 | cluster star |
| 9 | 260.2±5.0 | 15.24 | 1.58 | cluster star |
| 10 | 277.6±9.8 | 16.47 | 1.36 | cluster star |
| 11 | 279.4±3.4 | 16.56 | 1.52 | cluster star |
| 12 | 275.3±2.7 | 15.74 | 1.08 | cluster star |
| 13 | 284.0±2.5 | 16.35 | 1.35 | cluster star |
| 14 | 280.4±3.5 | 16.35 | 1.97 | cluster star |
| 15 | 235.1±4.2 | 16.11 | 1.44 | field star |
| 16 | 318.5±2.7 | 16.53 | 0.78 | variable/binary? |
| 17 | 275.2±3.6 | 16.82 | 1.15 | cluster star |
| 18 | 238.3±3.6 | 16.67 | 1.80 | field star |
| 19 | 206.9±2.7 | 16.56 | 1.33 | field star |
| 20 | 14.4±3.2 | 16.05 | 1.00 | foregr. star |
| 21 | 229.0±3.3 | 15.32 | 2.02 | field star |
| 22 | 84.3±3.4 | — | — | foregr. star |

**Table 6.** Observational parameters used to create artificial star clusters

| cluster | total mass [$M_\odot$] | number of stars | halfmass radius [pc] | tidal radius [pc] |
|---|---|---|---|---|
| SL 353 | 7300 | 20100 | 6.6 | 23.0 |
| SL 349 | 4800 | 13100 | 3.3 | 20.6 |

## 7. N-body simulations

Whether two clusters are interacting or not is hard to decide on the base of imaging data. According to de Oliveira et al. (1998) encounters of star clusters can be traced using isodensity maps. However, the field in which the clusters are embedded may likely influence the isopleths, and the distinction between field and cluster stars is a difficult task (Leon et al. 1999).

Assuming a Kroupa IMF (Kroupa et al. 1993) we estimate the total masses, the number of stars, and the half-mass and tidal radii of the star clusters SL 353 and SL 349. The observational parameters can be found in Table 6.

Based on a King model and the parameters listed in Table 6 two artificial star clusters were created which resemble the observed ones. Fig. 7 shows the density plot of the two artificial clusters placed at the same distance as the projected separation between the cluster pair SL 353 & SL 349 (18.1 pc). The star density between the clusters, where the density profiles are overlapping, is enhanced.

In order to get an idea whether an interacting cluster pair could be discerned from a mere overlap by chance in the line-of-sight, we performed N-body simulations using the GRAPE3a special purpose board in Kiel. The equations of motion were integrated using the standard leapfrog scheme with a constant time step of 0.15 Myr. Additionally, we allowed for a Plummer softening with a softening length of 0.1 pc. Since we assume that the cluster pair SL 353 & SL 349 is a 'real' pair we chose a parabolic orbit as a limiting case to unbound pairs. In case of a 'true' gravitationally bound cluster pair, one would expect elliptic orbits and, thus, a series of repetitive encounters which should result in even stronger signatures of an interaction or eventually already in a merger. At the beginning we started with a well detached system at a separation of 100 pc. The minimum distance (reached at t=0) was set to 12 pc. The simulation was stopped at separation of 18.1 pc, i.e. 13.4 Myr after closest approch. For simplicity, the tidal field of the parent galaxy is not considered in this simulation. Fig. 6 shows a face-on view of both clusters.

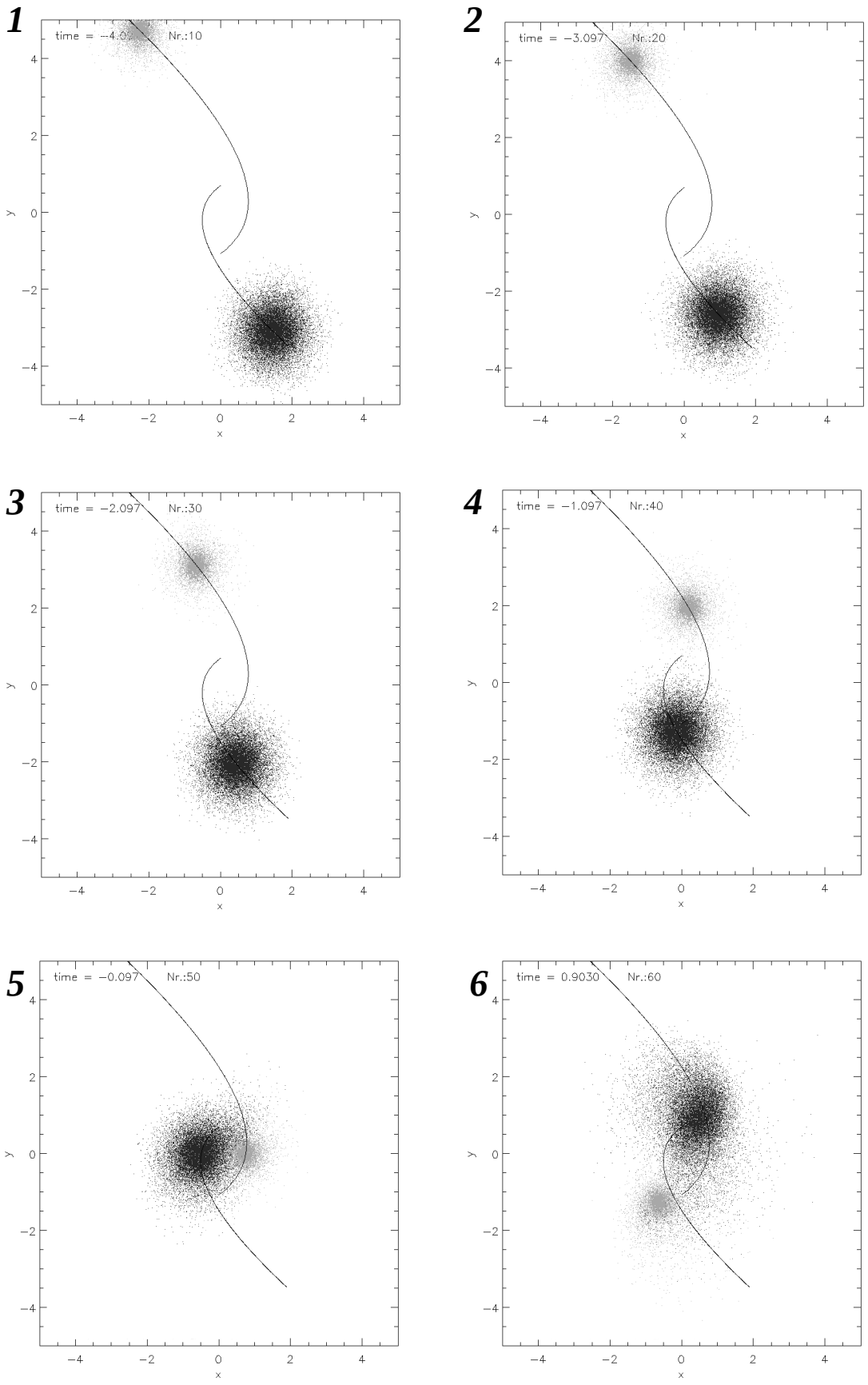


**Fig. 6.** N-body simulation of a close encounter of two star clusters which resemble our observed cluster pair. The two clusters approach each other on elliptical orbits under the influence of their gravitational forces. The tidal field of the parent galaxy is not considered in this simulation

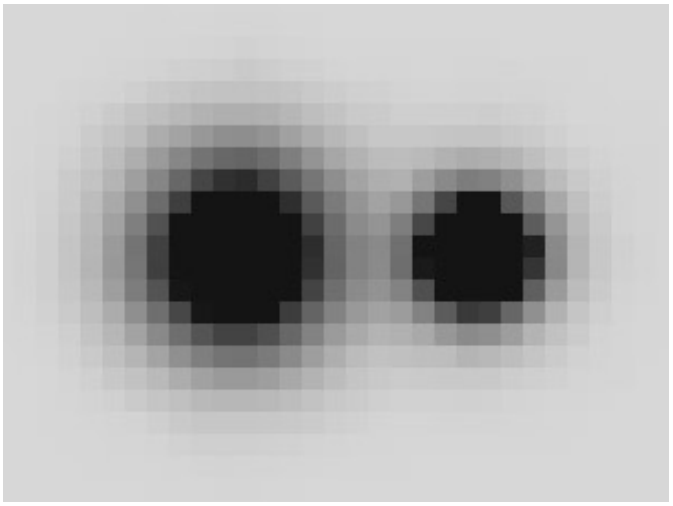

**Fig. 7.** Density plot of two artificial star clusters without any interaction. The centre-to-centre separation between the clusters is the same as the projected distance between the observed pair SL 353 & SL 349 (18.1 pc). The star density between the clusters, where the density profiles are overlapping, is enhanced

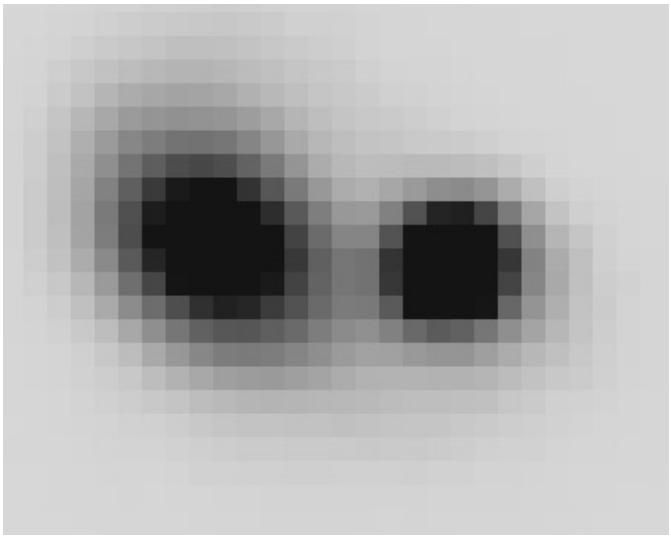

**Fig. 8.** Isopleth of the two artificial clusters with interaction, the distance between the two clusters is the same as in Fig. 7. The region between the clusters shows enhanced star density. The larger cluster shows a distortion while the smaller but more compact one remains mainly undisturbed in the isopleth

The isopleth of the interacting clusters, again at a distance of 18.1 pc, is presented in Fig. 8. Again, a region of enhanced star density connects both clusters. Furthermore the larger cluster shows a distortion while the smaller but more compact one remains mainly undisturbed in the isopleth. The density plot of the observed cluster pair (Fig. 2) shows a similar, northeast to south distortion around the more massive cluster SL 353. However, the observed northern distortion and the distortion of the smaller cluster SL 349 are not seen in Fig. 8.

We want to emphasize that the parameters used to create the artificial clusters are based on our observations, but are only estimates and should not be taken as strict values. The simulations are meant for qualitative comparison and a more detailed simulation is barely possible since the parameter space cannot be further restricted on the base of our data.

## 8. Summary and conclusions

Fitting isochrones based on the Geneva models (Schaerer et al. 1993) to the CMDs, we find that the components of the double cluster SL 353 & SL 349 are coeval within the accuracy of our data, and we derive an age of 550±100 Myr for both clusters.

The clusters are sufficiently old that the Ca II triplet visible in the spectra of red giants could be used to derive radial velocities. 22 stars in and around the two star clusters were investigated. Most stars located inside the cluster areas show similar velocities of $\approx 277 \pm 7\,\mathrm{km\,s^{-1}}$ whereas almost all field stars show lower velocities of $\approx 240 \pm 19\,\mathrm{km\,s^{-1}}$. Two foreground stars were identified through their velocities which are too low to belong to the LMC population ($14\,\mathrm{km\,s^{-1}}$ and $84\,\mathrm{km\,s^{-1}}$, respectively).

Both components of the binary cluster candidate are of the same age and, furthermore, have very similar mean radial velocities of $\approx 274 \pm 10\,\mathrm{km\,s^{-1}}$ for SL 349 and $\approx 279 \pm 4\,\mathrm{km\,s^{-1}}$ for SL 353. These findings support that both clusters may have formed at similar times and from the same GMC. In this sense they may constitute a true binary cluster.

We investigate the stellar densities in and around the binary cluster SL 353 & SL 349 and find an enhanced density between the two clusters. The smaller cluster SL 349 shows a distortion towards SL 353, and similar distortions can be seen around the more massive cluster.

Vallenari et al. (1998) found a distortion of the isophotal contours, similar to our Fig. 2, and a twisting of the isopleths which they regard as a sign of interaction and physical connection between the two clusters. It is remarkable that the age of this binary cluster is higher than the theoretical survival time of few $10^7$ yrs for physically connected cluster pairs suggested by Bhatia (1990). Leon et al. (1999) suggest that SL 349 & SL 353 are part of a larger star cluster group in which interacting binary clusters are formed later via tidal capture, thus explaining an age larger than the theoretical survival time. However, another explanation could be that the survival time might be larger in the LMC bar where the tidal field might be weaker, as proposed by Elson et al. (1987, their Fig. 13).

Whether the distortion of the clusters is indeed a sign of possible interaction cannot be decided on the basis of our imaging data alone.

Based on observational parameters we created two artificial star clusters. The isopleths of the non-interacting pair as well as of a simulated interacting pair of star clusters were compared with the observed density plot. The density plot of the artificial, interacting pair shows a distortion of the more massive cluster which can also be found in the observed isopleth, however, the observed distortion of the smaller cluster SL 349 is not seen in the artificial density plot. It seems likely that this cluster pair

shows signs of interaction, however, this does not necessarily imply that both clusters are gravitationally bound.

*Acknowledgements.* We would like to thank Prof. H. Elsässer for allocating time at the MPIA 2.2m-telescope at La Silla during which our imaging data were obtained, Hardo Müller for software advice, Klaas S. de Boer and Jörg Sanner for a critical reading of the manuscript. AD thanks Lick Observatory for their hospitality, where part of this work was done. This work was supported by a graduate fellowship of the German Research Foundation (Deutsche Forschungsgemeinschaft – DFG) for AD through the Graduiertenkolleg 'The Magellanic System and Other Dwarf Galaxies' (GRK 118/2-96). EKG gratefully acknowledges support by NASA through grant HF-01108.01-98A from the Space Telescope Science Institute, which is operated by the Association of Universities for Research in Astronomy, Inc., under NASA contract NAS5-26555. The simulations were carried out on the GRAPE3af special purpose computer in Kiel (DFG Sp345/5). This research has made use of NASA's Astrophysics Data System Abstract Service and of the SIMBAD database operated at CDS, Strasbourg, France.

## References

Bhatia R.K., 1990, PASJ 42, 757
Bhatia R.K., McGillivray H.T., 1988, A&A 203, L5
Bhatia R.K., Hatzidimtriou D., 1988, MNRAS 230, 215
Bhatia R.K., Read M.A., Hatzidimtriou D., Tritton S., 1991, A&AS 87, 335
Bica E., Claria J.J., Dottori H., Santos J.F.C. Jr., Piatti A.E., 1996, ApJS 102, 57
Brocato E., Buonanno R., Castellani V., Walker A.R., 1989, ApJS 71, 25
Brocato E., Castellani V., Piersimoni A.M., 1994, A&A 290, 59
de Oliveira M.R., Dottori H., Bica E., 1998, MNRAS 295, 921
de Oliveira M.R., Bica E., Dottori H., 2000, MNRAS 311, 589
Dieball A., Grebel E., 1998, A&A 339, 773
Efremov Y., Elmegreen B., 1998, MNRAS 299, 588
Ehlerová S., Palouš J., Theis C., Hensler G., 1997, A&A 328, 12
Ellingson E., 1989, A User's Guide to Multislit Spectroscopic Reductions with IRAF. ftp://iraf.noao.edu/iraf/docs/
Elmegreen B.G., Efremov Y.N., Pudritz R.E., Zinnecker H., 1999, to be published in: Mannings V.G., Boss A.P., Russell S.S. (eds.) Protostars and Planets IV, astro-ph/9903136
Elson R.A.W., Fall M., Freeman K.C., 1987, ApJ 323, 54
Evans D.S., 1967, In: Batten A.H., Heard J.F. (eds.) IAU Symp. No. 30, p. 57
Fischer P., Welch D.L., Mateo M., 1993, AJ 105, 938
Fujimoto M., Kumai Y., 1997, AJ 113, 249
Geisler D., 1990, PASP 102, 344
Grebel E., Roberts W.J., 1995, A&AS 109, 293
Grebel E.K., Roberts W.J., Brandner W., 1996, A&A 311, 470
Hatzidimitriou D., Bhatia R.K., 1990, A&A 230, 11
Kontizas E., Kontizas M., Xiradaki E., 1989, Ap&SS 156, 81
Kroupa P., Tout C.A., Gilmore G., 1993, MNRAS 262, 545
Lattanzio J.C., Vallenari A., Bertelli G., Chiosi C., 1991, A&A 250, 340
Leon S., Bergond G., Vallenari A., 1999, A&A 344, 450
Luck R.E., Lambert D.L., 1992, ApJS 79, 303
Olszewski E.W., Schommer R.A., Suntzeff N.B., Harris H.C., 1991, AJ 101, 515
Page T., 1975, In: Stars & Stellar Systems Vol. 9, University of Chicago Press, Chicago, p. 541
Prévot L., Andersen J., Ardeberg A., et al., 1985, A&AS 62, 23
Ratnatunga K., Bahcall J., 1985, ApJS 59, 63
Roberts W.J., Grebel E.K., 1994, American Astronomical Society Meeting #185, 104.02
Russell S.C., Bessell M.S., 1989, ApJS 70, 865
Russell S.C., Dopita M.A., 1992, ApJ 384, 508
Schaerer D., Meynet G., Maeder A., Schaller G., 1993, A&AS 98, 523
Schwering P.B.W., Israel F.P., 1991, A&A 246, 231
Searle L., Wilkinson A., Bagnuolo W., 1980, ApJ 239, 803
Stetson P.B., 1991, In: Grosbøl P.J., Warmels R.H. (eds.) 3rd ESO/ST-ECF Garching - Data Analysis Workshop, p. 187
Subramaniam A., Sagar R., 1999, AJ 117, 937
Sugimoto D., Makino D., 1989, PASJ 41, 991
Surdin V.G., 1991, Ap&SS 183, 129
Theis C., 1998, In: Duschl W., Einsel Ch. (eds.) Dynamics of Galaxies and Galactic Nuclei. Proc. Ser. I.T.A. Vol. 2, p. 223
Theis C., Ehlerová S., Palouš J., Hensler G., 1997, Proceedings of IAU Coll. 166, The Local Bubble and Beyond. Garching, p. 409
Thévenin F., Jasniewicz G., 1992, A&A 266, 85
Turnshek D.E., Turnshek D.A., Craine E.R., Boeshaar P.C., 1985, A&AS Vol. 1
Vallenari A., Aparicio A., Fagotto F., Chiosi C., 1994a, A&A 284, 424
Vallenari A., Aparicio A., Fagotto F., et al., 1994b, A&A 284, 447
Vallenari A., Bettoni D., Chiosi C., 1998, A&A 331, 506
van den Bergh S., 1996, ApJ 471, L31
Westerlund B.E., 1997, The Magellanic Clouds. Cambridge University Press, Cambridge, UK